Article

Densification of Ceramic Matrix Composite Preforms by Si$_2$N$_2$O Formed by Reaction of Si with SiO$_2$ under High Nitrogen Pressure. Part 2: Materials Properties

Brice Taillet, René Pailler and Francis Teyssandier *

Laboratoire des Composites ThermoStructuraux (LCTS), UMR 5801, CNRS, CEA, Safran, Université de Bordeaux, 33600 Pessac, France; brice.taillet@yahoo.fr (B.T.); pailler@lcts.u-bordeaux.fr (R.P.)
* Correspondence: teyssandier@univ-perp.fr

Abstract: Ceramic matrix composites (CMCs) have been prepared and optimized as already described in part I of this paper. The fibrous preform made of Hi-Nicalon S fibers was densified by a matrix composed of Si$_2$N$_2$O prepared inside the CMC by reacting a mixture of Si and SiO$_2$ under high nitrogen pressure. This part describes the oxidation resistance and mechanical properties of the optimized CMC. The CMC submitted to oxidation in wet oxygen at 1400 °C for 170 h exhibited an oxidation gradient from the surface to almost the center of the sample. In the outer part of the sample, Si$_2$N$_2$O, Si$_3$N$_4$ and SiC were oxidized into silica in the cristobalite-crystallized form. The matrix microstructure looks similar to the original one at the center of the sample, while at the surface large pores are observed and the fiber/matrix interphase is consumed by oxidation. The elastic modulus and the hardness measured at room temperature by nano-indentation are, respectively, 100 and 8 GPa. The elastic modulus measured at room temperature by tensile tests ranges from 150 to 160 GPa and the ultimate yield strength from 320 to 390 MPa, which corresponds to a yield strain of about 0.6%. The yield strength identified by acoustic emission is about 40 MPa.

Keywords: ceramic matrix composite; corrosion and oxidation; mechanical testing

1. Introduction

Ceramic matrix composites (CMC) have been designed and developed for extreme operating environments: high temperatures, mechanical stress, oxidizing atmospheres and in some cases even irradiation [1]. These materials are very efficient; however, they are expensive, partly due to the price of the high-performance fibers used to weave the preform, but also because of the chemical vapor infiltration process used to carry out the matrix densification of the preform. Alternative processes have been sought to lower the cost of CMCs. In situ densification of the preform by Si$_2$N$_2$O, processed by reacting Si, SiO$_2$ and N$_2$ under high nitrogen pressure, has been developed and detailed in part 1 of this paper. The present paper is devoted to the properties—mainly mechanical properties and resistance to oxidation—of the CMC optimized in part 1.

Since detailed description of the preform preparation and its subsequent densification is already published in part 1, only the basic features of these steps are recalled hereafter.

The fibrous preform manufactured by Safran Ceramics was made of Hi-Nicalon S fibers woven in a 3D interlock weave. A thin layer of pyrocarbon was first deposited at the surface of the fibers by chemical vapor infiltration (CVI). The preform was then pre-densified by a few-micrometer-thick layer of ß-SiC. Such a layer, which acts as a consolidation layer, provides the stiffness required for the handling of the preform. Two typical thicknesses of ß-SiC were used: 1 and 5 μm, corresponding to an open porosity of 53 and 35% respectively. The as-prepared preforms were eventually submitted to a densification reaction aimed at forming a matrix composed of Si$_2$N$_2$O. For that purpose, a mixture of Si and SiO$_2$ powders in the ratio 3/1 corresponding to balance Equation (1) was

impregnated into the preform by suction of submicron powder slurry. A modification of the process, consisting in the formation of silica inside the preform by oxidizing in situ part of the impregnated silicon, was also tested. In this modified process, the volume increase caused by the transformation of silicon into silica improves the densification of the matrix.

$$3\,Si + SiO_{2\,(s)} + 2\,N_{2\,(g)} \rightarrow 2\,Si_2N_2O \tag{1}$$
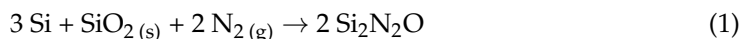
The reaction was initiated by increasing the temperature of the powder till a critical value. Heating of the samples was carried out by means of a resistor made of 2D carbon/carbon composite material provided by Safran Ceramics, which was wrapped around the samples but not in direct contact with them. The Joule-heated resistor was disposed inside a vessel made of 316L inox and designed to withstand a pressure of 20 MPa. The reaction took place in the presence of nitrogen: three pressures (1, 2 and 3 MPa) were tested.

In view of the final applications of CMC, both the resistance against oxidation at high temperature in moist air and mechanical properties, but at room temperature, were tested.

Oxidation of SiC and Si$_2$N$_2$O

The processed matrix is mainly composed of Si_2N_2O but also includes Si_3N_4, which is formed in competition with Si_2N_2O during the synthesis reaction. Two allotropic crystalline forms of each compound were identified in the matrix by X-Ray diffraction (XRD). The proportion of each form is presented and discussed in part 1 of this paper; only the global ratio of the two compounds is given here.

Oxidation of the CMC materials may affect both the matrix and the consolidated preform. In the matrix, both Si_2N_2O and Si_3N_4 can be oxidized. SiC is present in both the fibers of the woven preform and in the consolidation layer. Oxidation of silicon carbide (SiC) has been extensively studied. SiC is an oxidation-resistant material at high temperatures due to its ability to form a continuous protective oxide scale (SiO_2) under highly oxidative environments (passive oxidation). However, at very high temperatures and/or under less oxidative environments, the oxidation of SiC leads to the formation of gaseous products, such as SiO(g) and CO(g) instead of a protective scale (active oxidation). These oxidation conditions do not protect the material and have a detrimental effect on it [2,3]. Moreover, even under passive oxidation conditions, the protective SiO_2 scale can volatilize in the presence of water vapor, due to the formation of mainly two silicon hydroxide species: $Si(OH)_4$ and $SiO(OH)_2$ [4].

A whole body of research has also been devoted to the oxidation of Si_3N_4 in dry oxygen. In our case, oxidation of Si_3N_4 may take place either by reaction between SiO_2 and Si_3N_4 or by reaction with molecular oxygen in equilibrium with SiO_2. The isothermal section of the ternary Si-N-O phase diagram (see part I) shows that Si_2N_2O is the equilibrium phase that should be formed by reaction between SiO_2 and Si_3N_4. However, based on annealing studies of thin film couples, Du et al. [5] have shown that the solid-state reaction between these two phases is extremely slow. In the same way as for SiC, the scale formed during oxidation follows parabolic oxidation kinetics; however, below 1500 °C the parabolic growth rate of the oxide scale on Si_3N_4 can be up to three orders of magnitude lower [6]. Ogbuji [7,8] has shown the presence of a SiOxNy amorphous layer between Si_3N_4 and SiO_2 when Si_3N_4 is oxidized. Such a layer, which is formed by progressive O-for-N substitution in the silicon oxynitride tetrahedral unit, is a better barrier than SiO_2 to oxygen diffusion because of a tighter network structure. In the range of 900 to 1000 °C, the presence of water vapor does not seem to significantly modify the oxidation processes, [9] but it is mainly expected to favor the reactive vaporization of the silica layer.

The oxidation of Si_2N_2O has been much less extensively studied. This oxide is usually considered to be more resistant to oxidation than Si_3N_4 or SiC [10]. The oxidation reaction forms a silica scale and nitrogen according to the following balance equation:

$$Si_2N_2O(s) + 3/2\,O_2(g) = 2\,SiO_2(s) + N_2(g) \tag{2}$$
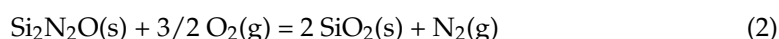
The oxidation kinetics vary considerably depending on the method of preparation used. In particular, the oxidation resistance of sintered materials is highly dependent on the sintering additives, which modify the protective properties of the formed oxide scale. Among articles dealing with the oxidation of Si_2N_2O, those of Lortholary et al. [11], Persson et al. [12] and Manessis et al. [13] are related to materials sintered without additives. Samples used by Lortholary et al. had been prepared from a mixture of silicon and silica ($Si/SiO_2 = 3$) heated at 1450 °C in a mixture of oxygen and argon ($Ar/O_2 = 2$). They observed that under an oxygen pressure of 42 kPa, oxidation starts at 800 °C but does not become significant until after 1000 °C. The silica formed remains amorphous below 1250 °C and crystallizes in the α-cristobalite form at higher temperatures. In the temperature range of 1100 to 1250 °C, the measured oxidation kinetics have been fitted by two successive oxidation laws. Sorption of atomic oxygen at the Si_2N_2O surface controls oxidation kinetics up to a silica thickness of 150 Å, while diffusion of oxygen through the silica scale is the limiting rate for higher thicknesses. The samples used by Persson et al. [12] and Manessis et al. [13] are formed by hot isostatically pressing (HIP) mixtures composed of equal molar amounts of high purity Si_3N_4 and SiO_2 powders heated at 1900 °C. They both contain about 2 wt% α-Si_3N_4 and 2 wt% ß-Si_3N_4. In the temperature range of 1000 to 1300 °C, Manessis et al. [13] observed that the oxidation rate is controlled by diffusion of O_2 through the amorphous silica scale and exhibits a parabolic behavior as a function of time. At higher temperatures (1300 to 1600 °C), Persson et al. [12] observed that silica begins to crystalize in the α-cristobalite form. If the time-dependent law is parabolic at 1300 °C, this is no longer the case above 1350 °C. These latter authors have determined that above 1350 °C, the oxidation law can be derived from a diffusion law of O_2 through the amorphous SiO_2 film in between the α-cristobalite crystals, the size of the latter increasing with temperature. It should also be noticed that Si_2N_2O can decompose well below its congruent melting point (1893 °C). Mass spectroscopic studies of its thermal behavior under a vacuum [14] have shown that it starts to decompose into SiO, N_2, and Si_3N_4 above 1000 °C. However, high SiO and/or N_2 pressures prevent such decomposition [15]. The nitrogen released during the oxidation process (balance Equation (2)) is evacuated through the silica scale, but the outward diffusion of N_2 through the silica scale does not seem to have an influence on the inward diffusion of O_2 [11,13].

We have not found any article dealing with the oxidation of Si_2N_2O in the presence of water vapor. Assuming that water vapor has no specific oxidation influence on Si_2N_2O, it should mainly affect the formed silica through enhanced SiO_2 vaporization by formation of gaseous hydroxides, as previously mentioned in the case of SiC oxidation.

2. Experimental Details

2.1. Oxidation Experiments

The oxidation of samples was carried out in a high-temperature furnace (Pyrox, Tmax = 1600 °C) associated with a water vapor saturator. Thanks to this device, the oxidation mixture was composed of 50 kPa air/50 kPa water vapor. The oxidation temperature was set at 1400 °C. The heating and cooling sequences were carried out under argon, the water vapor being introduced only during the temperature step. The total processing time was 170 h, but was split into several periods of time in order to characterize the samples at various oxidation states. At each stage of oxidation these characterizations included scanning electron microscopy (SEM FEI QUANTA 400 FEG V3 equipped with energy dispersive X-ray spectrometry (EDS)) observation of the sample's surface, weight variation measurement and identification by XRD (Bruker D8 advance equipped with copper anticathode Lambda $K_{\alpha1-2}$) of the crystalline species formed. The residual open porosity was also measured by mercury porosimetry using a Micromeritics Autopore IV 9500 porosimeter.

Two types of composite specimen were tested:

1. A preform A, in which a 1-µm-thick consolidation layer made of SiC was first deposited by CVD. The preform was further impregnated by suction of submicron

silicon powder slurry. Part of this silicon was finally oxidized in situ to provide the silica required for the Si_2N_2O synthesis reaction. The resulting composite matrix was composed of 90 wt% Si_2N_2O with the remaining 10% being Si_3N_4. The measured open residual porosity of the matrix was 20%.

2. A preform B, in which a 5-μm-thick consolidation layer made of SiC was first deposited by CVD. The preform was further impregnated by suction of submicron silicon/silica (3/1) powder slurry. The resulting composite matrix was composed of 75 wt% Si_2N_2O with the remaining 25% being Si_3N_4. The measured open residual porosity of the matrix was 14%.

2.2. Mechanical Testing

The stress tests were applied to composite materials processed under the same conditions:

-   SiC consolidation layer: 5 μm thick,
-   Powder mixture impregnated with a slurry composed of Si and SiO_2 ($Si/SiO_2 = 3$),
-   Reaction synthesis carried out with a heating rate of 200 °C/min and under a nitrogen pressure of 2 GPa,
-   In order to minimize the thermal residual stress, a cooling rate of 10 °C/min was imposed.

For a detailed description of the whole sample preparation and synthesis procedure, the reader is referred to part 1 of this paper.

The processed composite samples were subjected to nanoindentation and stress tests.

Local elastic modulus and microhardness were measured by nanoindentation. These measurements were performed by a NT600 device from Micro Materials Limited Company. This device is composed of a mechanical probe (triangular-base pyramidal berkovich indenter) associated with an optical microscope. Load application and displacement measurements were performed along a horizontal axis by means of a pendulum on which the indenter was attached. The tests were run at an indentation speed of 1 mN/s and a maximum load of 200 mN.

The elastic modulus as determined by the nanoindentation test is given by the following equation:

$$\frac{1}{E_r} = \frac{1 - v_i^2}{E_i} + \frac{1 - v^2}{E} \tag{3}$$

where: E_i and v_i are, respectively, the elastic modulus and the Poisson coefficient of the indenter; E and v are, respectively, the elastic modulus and the Poisson coefficient of the tested material; and E_r is the reduced modulus.

The indenter is made of diamond: E_i = 1141 GPa and v_i = 0.07.

When the elastic modulus of the material being tested is small as compared to the one of diamond, which is our case, the tip of the indenter can be considered as infinitely stiff and the contribution of the indenter in Equation (3) becomes negligible.

Therefore Equation (3) becomes:

$$\frac{1}{E_r} = \frac{1 - v^2}{E} \text{ or } E = E_r\left(1 - v^2\right) \tag{4}$$

As we did not know the Poisson coefficient of our material, we used the reduced modulus.

The stress tests were conducted at room temperature on an electromechanical-driven Instron 4505 testing machine equipped with self-tightening jaws. We used simple bar tensile samples (70 × 15 × 3.3 mm) with aluminum studs glued to the specimen. The longitudinal direction of the bar sample corresponds to the weft direction of the preform. The sample deformation was measured by knife extensometers. The tensile tests were carried out either at a constant rate of 0.05 mm/min or under cyclic traction at a constant rate of 0.1 mm/min. In the latter case, successive load/unload cycles were applied at increasing loads until the

specimen broke. During each mechanical test a piezoelectrical sensor was mounted on one of the jaws to detect the acoustic waves associated with material damage. A threshold of 45 dB was necessary to filter the ambient noise. Acoustic emission is a transient wave resulting from the sudden release of stored energy during a damage process. In composite materials, matrix cracking, fiber failure, interfacial debonding and sliding of the fibers in the matrix are possible sources of acoustic emission.

3. Results and Discussion

3.1. Oxidation Tests

The properties of the two samples tested are gathered in Table 1.

Table 1. Properties of samples A and B subjected to oxidation tests.

Sample Ref.	Thickness of the Consolidation Layer	Elaboration Conditions	Vol % Initial Open Porosity	Vol % Residual Open Porosity	Vol % of Matrix in the Sample	Wt % Si_2N_2O in the Matrix	Wt % Si_3N_4 in the Matrix	Wt % Si_2N_2O in the Sample	Wt % Si_3N_4 in the Sample
A	1 µm	200 °C/min 20 bar	53%	20%	33%	90%	10%	30%	3%
B	5 µm	200 °C/min 20 bar	33%	14%	19%	75%	25%	14%	5%

The oxidation conditions used (1400 °C in an air/water vapor mixture) were particularly severe. The change in physical appearance of the surface of the samples at different stages of oxidation is observed in Figure 1. The initial grey color is the color of Si_2N_2O. The more a sample is oxidized, the more its surface is covered with a whitish layer. This phenomenon is more pronounced for the sample with a 1-µm-thick consolidation layer, which is the one with the highest proportion of matrix material. The surface layer, as characterized by XRD using grazing incidence, is composed of crystalized silica in the cristobalite form, as expected due to the oxidation temperature. This characterization further reveals that the peaks belonging to cristobalite silica and ß-SiC are the only ones observed after an oxidation period of 22 h. Therefore, the Si_2N_2O and Si_3N_4 compounds, which are the preponderant constituents of the matrix, are totally transformed into SiO_2 at least in the thickness analyzed under grazing incidence. In contrast, the XRD analysis at normal incidence of the entire thickness of sample B (3.3 mm before (Figure 2) and after oxidation (Figure 3) shows that Si_2N_2O and Si_3N_4 compounds are still present in the bulk after the entire oxidation period (170 h). As expected, silicon carbide is predominant in the as-synthetized sample due to its presence in both the fibers and consolidation layer. SiO_2 is, as expected, the preponderant constituent after oxidation. Variation in the elemental composition was observed by electron dispersive spectroscopy (EDS) on a cross section of sample B oxidized for 170 h (Figure 4). It confirms the oxidation gradient of the sample, but furthermore reveals that the oxidation process affects a large proportion of the sample thickness. The SEM observation of the sample surface after an oxidation period of 170 h reveals the formation of flakes of silica layer and some degradation of the open-ended fibers (Figure 5). Modification of the silica layer is caused by its enhanced vaporization because of the presence of water vapor in the gas phase. The same characterization could not be obtained in sample A due to the disappearance of part of the matrix.
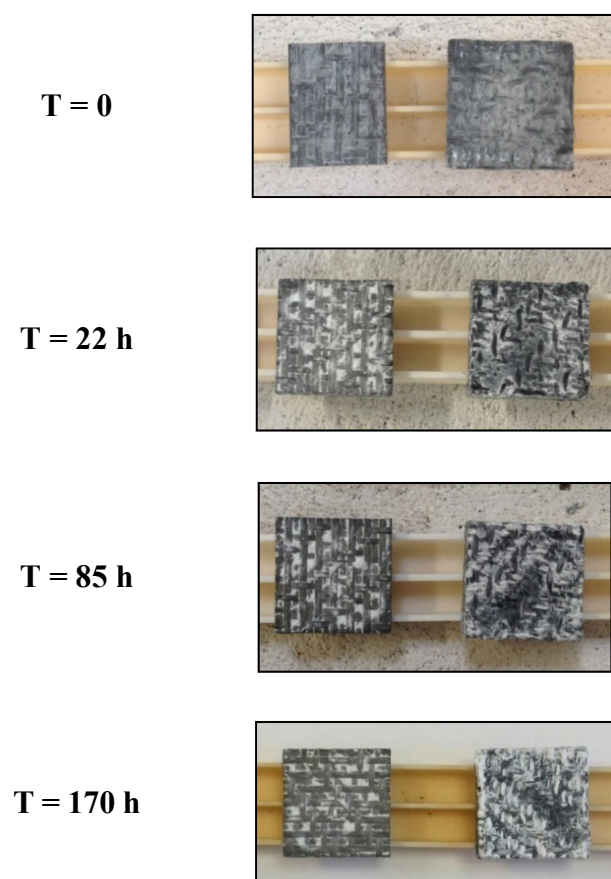
Figure 1. Photographs of composite samples after oxidation treatments in moist air. The consolidation SiC layer is 5 μm thick for sample B (left) and 1 μm thick for sample A (right).
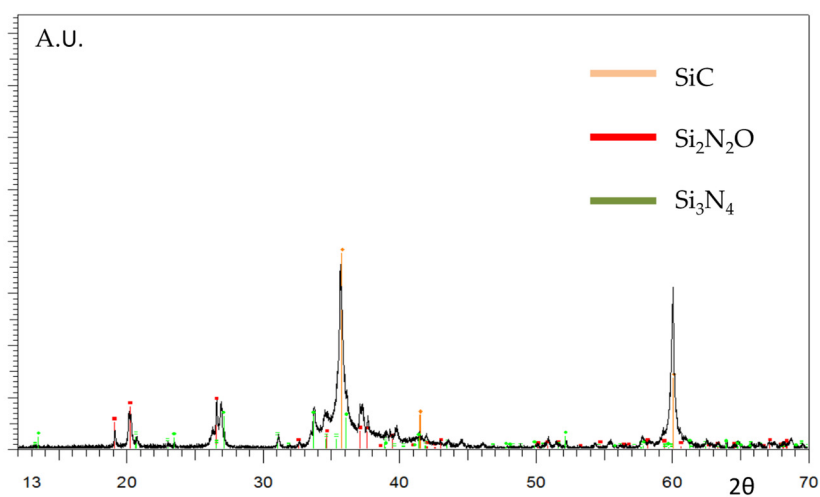

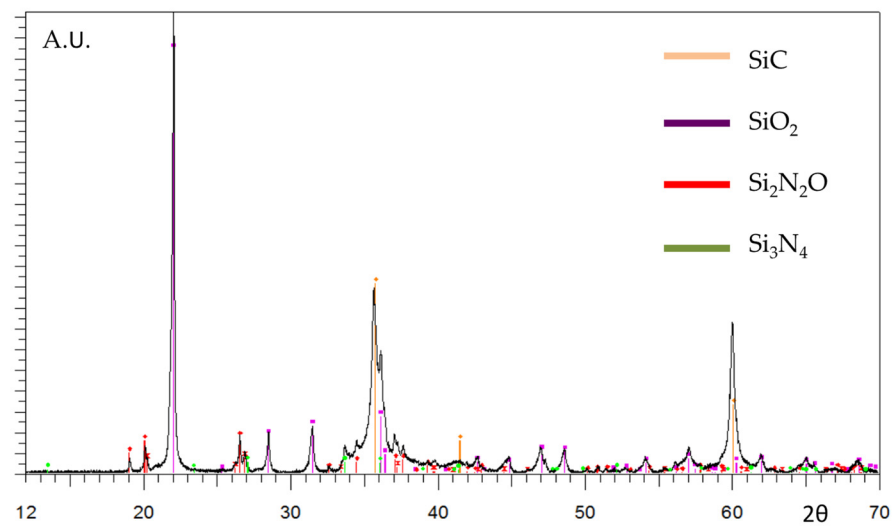**Figure 2.** XRD spectrum at normal incidence of the section of sample B as synthesized.

Figure 3. XRD spectrum at normal incidence of the section of sample B after oxidation for 170 h.
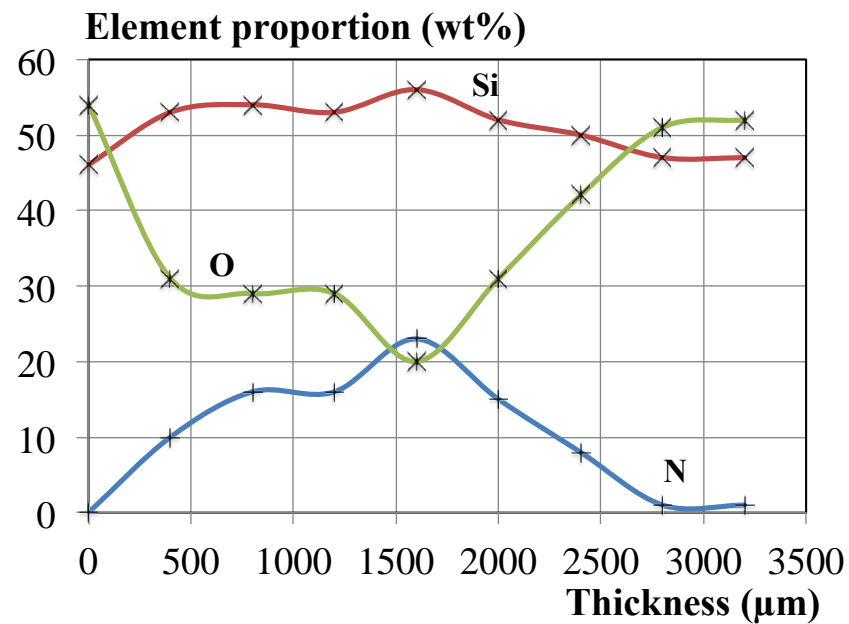

Figure 4. Variation in the elemental weight composition as characterized by EDS carried out on a cross section of oxidized sample B. Oxidation time 170 h, temperature 1400 °C, water partial pressure 50 kPa and SiC thickness 5 μm.
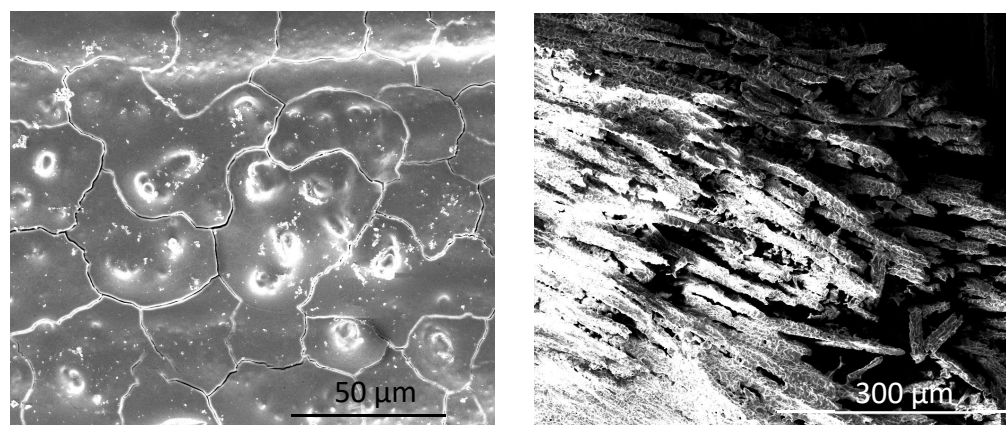
Figure 5. SEM photograph of the surface of sample B oxidized for 170 h. Left: silica layer. Right: open-ended fibers. Oxidation time 170 h, temperature 1400 °C, water partial pressure 50 kPa and SiC thickness 5 μm.

Figure 6 shows the variations in the weight increase divided by the surface of sample A and B, as measured at various time steps. The weight increase is high during the first 20 h for both consolidation layers. Such a period corresponds to the formation of the silica layer resulting from the surface oxidation of the samples (both matrix and fibers). Beyond an oxidation time of 40 h, the weight gain of sample B (5 μm) no longer increases, while it continues to increase for sample A (1 μm). This does not mean that the oxidation of sample B has stopped, but that the growth rate of the silica layer becomes equal to its vaporization rate, mainly provoked by the water vapor. The weight gain of sample A continues to increase up to 170 h. Beyond this period, a level of weight gain is also observed for this sample. The reasons for these differences in behavior are not immediately apparent. Indeed, we assumed when choosing to densify the matrix with Si_2N_2O that the oxidability of this material was lower than that of SiC or Si_3N_4. In fact, the oxidability of a material depends not only on its intrinsic qualities of resistance to oxidation, but also on its microstructure (grain size, porosity...). It is difficult to verify the nature of the predominantly oxidized phases in the matrix of the sample, which additionally exhibits an oxidation gradient. It can however be observed that the percentage of Si_2N_2O in the samples (Table 1) is twice as high in sample A than in sample B, and that the rate of oxidation is equal to the rate of vaporization for the two samples after 170 h. Figure 6 indicates that the weight gain of sample A is, at the end of this time, twice as high as that of sample B, which would tend to show that Si_2N_2O is preferentially oxidized in the two samples. As already discussed in the introduction, Persson et al. [12] observed that above 1350 °C, which is our case, the diffusion rate of Si_2N_2O is no longer controlled by the diffusion of oxygen through the silica layer but by the diffusion of O_2 through the amorphous silica that separates the cristobalite grains, which continue to grow. In our case, it is probable that the porosity of the matrix also favors the oxidation of Si_2N_2O.

In Figure 7, the SEM observation of the matrix microstructure after an oxidation time of 170 h reveals that the central part of the sample looks similar to the original matrix before oxidation, even though some porosity with a medium size of 500 nm has appeared. The fibers as well as the pyrocarbon interphase between the fiber and the matrix do not seem to be affected by the oxidation process, and the amount of elemental nitrogen measured by EDS is lower than that of the elemental oxygen. In contrast, near the surface, the medium size of the porosity is much larger (10 μm) and the pyrocarbon interphase between the fiber and the matrix, which is no longer observable, has probably been entirely oxidized. The nitrogen element is almost absent from the EDS spectrum.
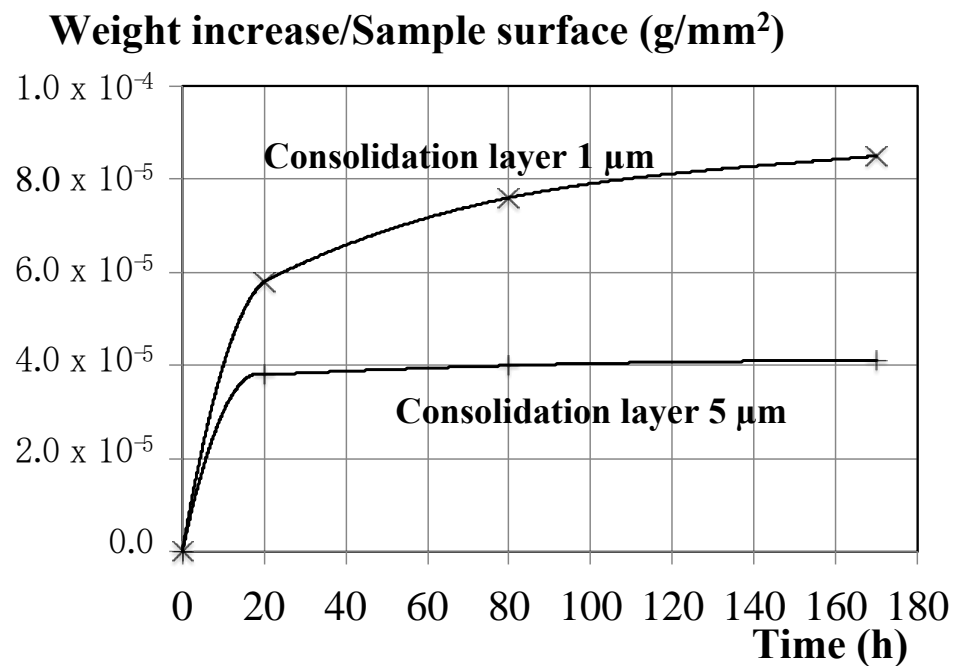
Weight increase/Sample surface (g/mm²)

Figure 6. Variation in the weight increase divided by the surface of the sample, as measured at various time steps for a preform consolidated either by a 1-µm-thick SiC layer (sample A) or by a 5-µm-thick SiC layer (sample B).
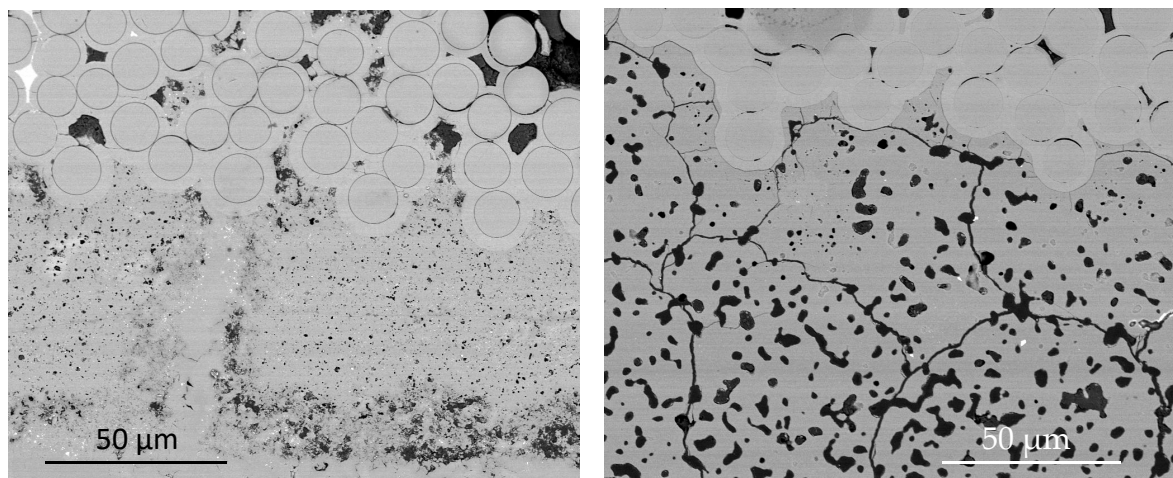

Figure 7. SEM photograph of a cross section of the composite sample B oxidized for 170 h. Left: core of sample. Right: near the surface. Oxidation time 170 h, temperature 1400 °C, water partial pressure 50 kPa and SiC thickness 5 µm.

3.2. Mechanical Tests

3.2.1. Indentation Test

For each sample, measurements were carried out in several places on the sample surface in order to check for the presence of inhomogeneity and take into account the dispersion of values due to the composite nature of the material.

The elastic modulus E and hardness value H measured for different matrix compositions are gathered in Table 2.

Table 2. Properties of the tested samples.

Sample N°	Thickness of the Sic Consolidation Layer	Pre-Oxidation of the Matrix before CS Processing	Elaboration Conditions	Composition (Weight %)	Residual Open Porosity	Reduced Modulus E_r (GPa)	Hardness H (GPa)
1	1 μm	-	200 °C/min 2 Mpa	95% Si_2N_2O 5% Si_3N_4	27%	101.2 +/− 6.3	8.4 +/− 1.1
2	1 μm	-	200 °C/min 3 Mpa	80% Si_2N_2O 20% Si_3N_4	28%	104.8 +/− 11.2	9.0 +/− 1.9
3	1 μm	1 h 15,900 h in air	300 °C/min 3 Mpa	85% Si_2N_2O 15% Si_3N_4	22%	99.7 +/− 7.4	8.1 +/− 1.3
4	5 μm	-	200 °C/min 2 Mpa	80% Si_2N_2O 20% Si_3N_4	16%	71.8 +/− 4.5	5.5 +/− 0.7
5	5 μm	-	300 °C/min 3 Mpa	65% Si_2N_2O 30% Si_3N_4 5% Si	13%	67.0 +/− 7.4	4.3 +/− 1.2

The measured values are much lower than the theoretical values relating to Si_2N_2O or Si_3N_4. These latter values are, respectively, 230 GPa, 10 GPa, 320 GPa and 14 GPa. The measured values are even lower when the consolidation layer is 5 μm thick, in spite of a reduced residual open porosity. We can also notice the dispersion of the measured values, reflecting the inhomogeneity of the matrix. Therefore, taking into account the dispersion of measurements, both the elastic modulus and the hardness can be considered to be the same for a given thickness of consolidation layer, regardless of the matrix composition or its porosity. Indeed, when the thickness of the consolidation layer is chosen, neither the matrix composition nor the residual open porosity vary significantly with the preparation conditions. As already emphasized in part 1 of this paper, when the SiC consolidation layer is thick (5 μm) the amount of impregnated powder introduced into the preform is lowered by 30 to 40%, and the powder no longer fills the intra-tow porosity. As a consequence, both the lower amount of powder introduced into the preform and the increased amount of SiC, which acts as a thermal sink, contribute to dampening the synthesis reaction and lowering its exothermicity. In a logical way, the SiC thickness is the parameter that most affects both the hardness and elastic modulus.

When the composite material is consolidated with a 1-μm-thick SiC layer, the SEM observation of the Berkovitch print shows some porosity in the left photograph of Figure 8. The pore size ranges between 200 and 300 nm. When the composite material is consolidated with a 5-μm-thick SiC layer, the matrix is rather inhomogeneous and seems to be less bound in some places (right photograph in Figure 8). The residual open porosity measured by mercury porosimetry is, in this case, centered on 100 nm.

3.2.2. Stress Test

The matrix obtained after reaction was composed of 75 wt% Si_2N_2O and 25 wt% Si_3N_4, and the amount of residual silicon was less than 1 wt%. The open residual porosity as measured by mercury porosimetry was 15%.

The test sample was cut out of a preform to the following size: 70 ∗ 30 ∗ 3.3 mm. It was then impregnated with a slurry and eventually processed into the reactor. After reaction, the test sample was cut into two identical samples (70 ∗ 15 ∗ 3.3 mm) and the aluminum studs were glued to each specimen. The measured properties of two identically processed samples are gathered in Table 3.

Table 3. Measured mechanical properties of two composite materials identically processed and submitted to tensile tests at a constant rate of 0.05 mm/min.

Sample	E (Gpa)	σ_e (MPa)	σ_r (MPa)	ε_r (%)
1	143 ± 3	40–45	323	0.5
2	147 ± 3		336	0.51

The stress-deformation curves, together with the cumulated number of events recorded by acoustic emission during the tensile test, are plotted in Figure 9. The stress-deformation curves are close together, reflecting a good reproducibility of the material behavior. Such curves are typical for CMC tensile stress behavior [16]. They are composed of several parts corresponding to specific damages of a composite material. The first linear part (I) corresponds to the elastic behavior of the material up to 40 MPa, during which the acoustic emission is low. During the second part (II), increasing amounts of acoustic events are recorded, which are emitted by the cracks generated in the matrix perpendicularly to the loading direction. These cracks are stopped by the fibers and deflected at the interface between the fiber and the matrix. These phenomena are responsible for the debonding of the fibers from the matrix. When both the matrix cracking and the fiber debonding are complete, the load becomes carried essentially by the fibers within the tows (part III starting at about 200 MPa). The mechanical behavior in this domain is controlled by the fiber tows oriented in the load direction. As the load increases, the fibers begin to fail individually. When the surviving fibers cannot carry the load increment resulting from a fiber failure, an increasing amount of fibers fail, which generates a rapid increase in the acoustic events. The failure of the tow then occurs, eventually causing ultimate composite failure.
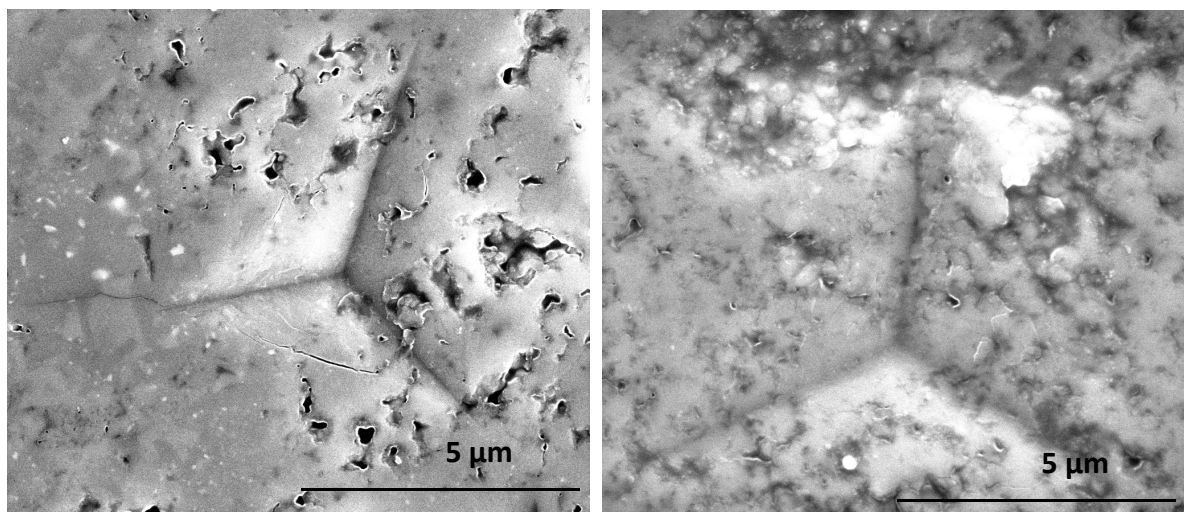

Figure 8. SEM photograph of a Berkovitch print in a matrix. Left: composite material consolidated with a 1-μm-thick SiC layer. Right: composite material consolidated with a 5-μm-thick SiC layer. Oxidation time 170 h, temperature 1400 °C, water partial pressure 50 kPa and SiC thickness 5 μm.
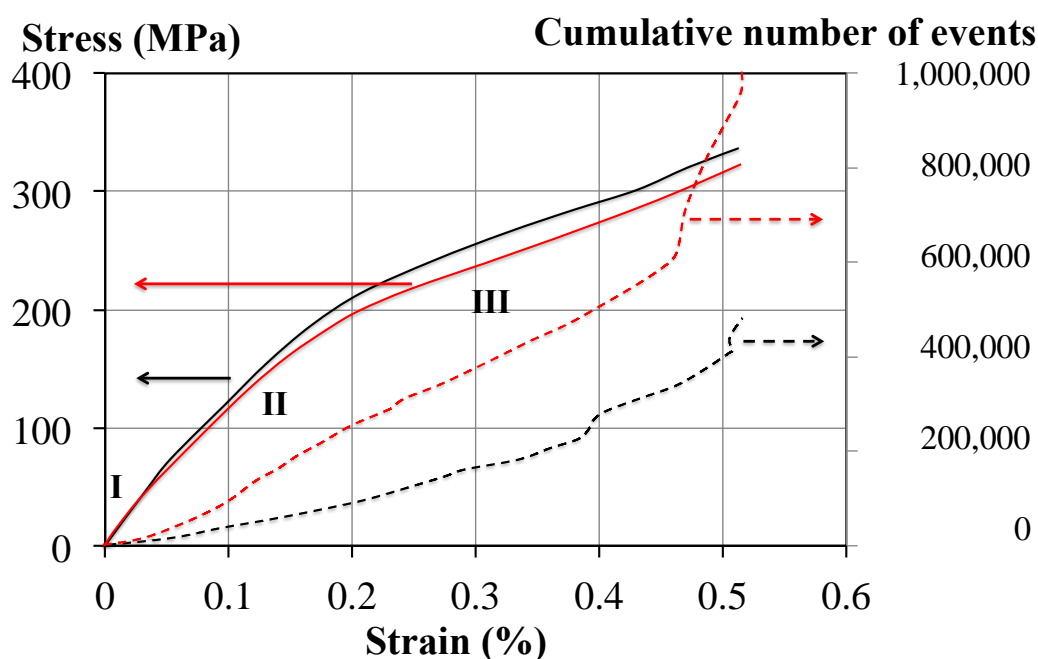
Figure 9. Stress-deformation curves together with the cumulated number of events recorded by acoustic emission during the tensile test. The black lines correspond to sample 2 (Table 3). The red lines correspond to sample 1 (Table 3).

The measured properties (elastic limit σ_e, ultimate tensile strength σ_r, yield strain (elongation at failure) ε_r and elastic modulus E) are gathered in Table 3 for two samples processed identically. The elastic modulus and elastic limit, respectively 145 GPa and 40 MPa, are rather low as compared, for instance, to an A40C CMC, which has the following mechanical characteristics: elastic modulus of 190 GPa and elastic limit of 95 MPa. Therefore, the matrix damage of our material starts at a relatively low load. Much of this difference can be attributed to the presence of the matrix porosity whose medium size lies in the range of 200 to 300 nm. These macropores are preferential locations to initiate cracks because they are places of stress concentration. This analysis is also in good agreement with the nanoindentation tests carried out on the matrix. Using a law of mixture, they revealed a Young's modulus lower than that expected compared to solid ceramics (Si_2N_2O, Si_3N_4). The yield strain of our composite material is also smaller than the one of an A40C CMC, but this only reflects the higher stiffness of the Hi-Nicalon S fibers (third generation Nicalon fiber) as compared to the Nicalon fiber (first generation Nicalon fiber) used in A40C. It can also be noticed that the high temperature encountered by the fibers during the reaction synthesis does not seem to modify their mechanical properties, as the ultimate tensile strength of our CMC is in agreement with the expected value of a CMC built from a Hi-Nicalon S preform. Protection of the fibers by a 5-µm-thick SiC layer should also contribute to this result.

3.2.3. Cycled Tensile Test

The mechanical properties of the test sample are the following:

- Elastic modulus: 158 ± 3 GPa
- Elastic limit: 40 ± 3 MPa
- Ultimate tensile strength: 350 MPa
- Yield strain: 0.59

The stress-strain curve presented in Figure 10 was obtained by a cycled tensile test after six load–unload cycles till the failure of the composite material. As expected, the cumulative number of acoustic events increases with strain. It can be noticed that in the last part of the cumulative number of acoustic events at the end of the last loading cycle, the peculiar variation in the number of acoustic events is indicative of the close failure

of the composite material. Damage to the composite before it breaks is mainly linked to multiple cracking of the matrix and associated mechanisms such as interfacial decohesion, fiber/matrix slippage or load transfers.
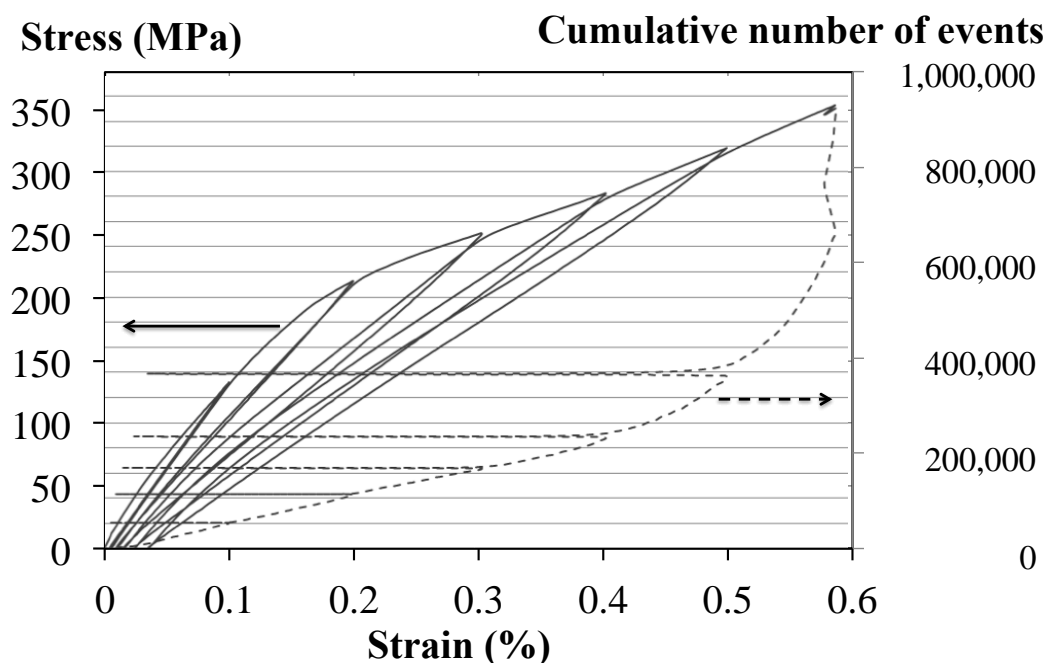

Figure 10. Stress-deformation curves corresponding to a cycled tensile test (solid line) together with the cumulated number of events (dotted line) recorded by acoustic emission during the tensile test.

The opening of the hysteresis loops (Figure 11) provides information about the sliding and deterioration at the fiber–matrix interface in the damaged areas of the composite. It is measured at the full width of a loop at its half maximum Figure 10. During the loading of the composite, the sliding at the fiber–matrix interface results in the formation of a crack network in the matrix. At the time of unloading, the cracks close and many of the fibers slide back into their original locations. However, in the damaged areas some fibers do not slide back into their original locations which leads to some residual deformation: the larger the hysteresis loop, the lower the magnitude of the friction force between the fiber and the matrix during the sliding of the fiber; the higher the difference at zero load between the deformation at the beginning and at the end of the loop, the higher the residual deformation. The enhanced increase of the loop opening observed at 220 MPa corresponds to the beginning of the fiber failures and the inter-tow delamination. In the present composite material, the maximum residual deformation ($\varepsilon = 0.037$) is about 6% of the yield strain, while it represents 15% in the case of an A40C CMC. These results show that the fiber–matrix interface plays its full part.

We also looked at variation in the elastic modulus as a function of the maximum load applied (Figure 12) and thus as a consequence of the damage undergone by the CMC. Variation in the elastic modulus has been approximated by the secant modulus of the hysteresis loops, which is defined by the ratio between the maximum stress applied during the loop and the corresponding deformation reduced by the initial deformation at the beginning of the loop. When the applied stress is higher than the value for which the matrix is saturated with cracks, both the opening of the hysteresis loop and secant modulus tend towards an asymptotic value. The increase in the amount of damaged fibers is responsible for a decrease in the composite stiffness and a sharp increase in both the opening of the hysteresis loops and residual deformation (Figure 13).
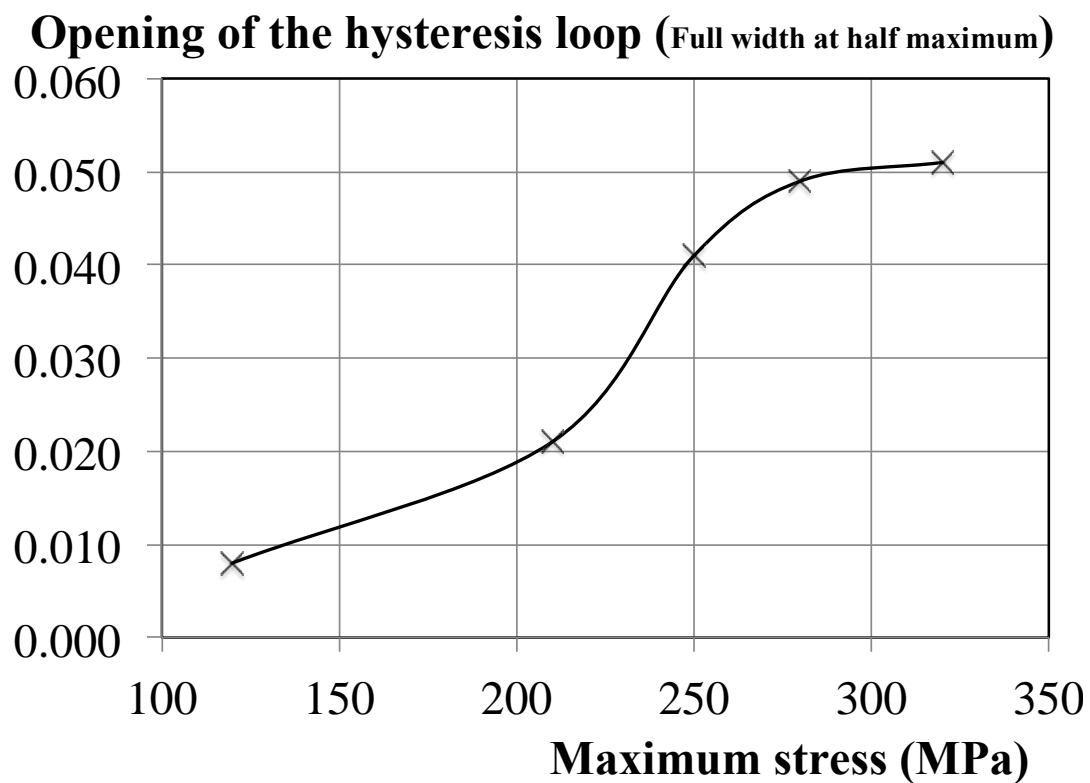
Opening of the hysteresis loop (Full width at half maximum)

Figure 11. Variation in the opening of the hysteresis loops of a given cycle as a function of the maximum stress imposed to the test piece during this cycle.
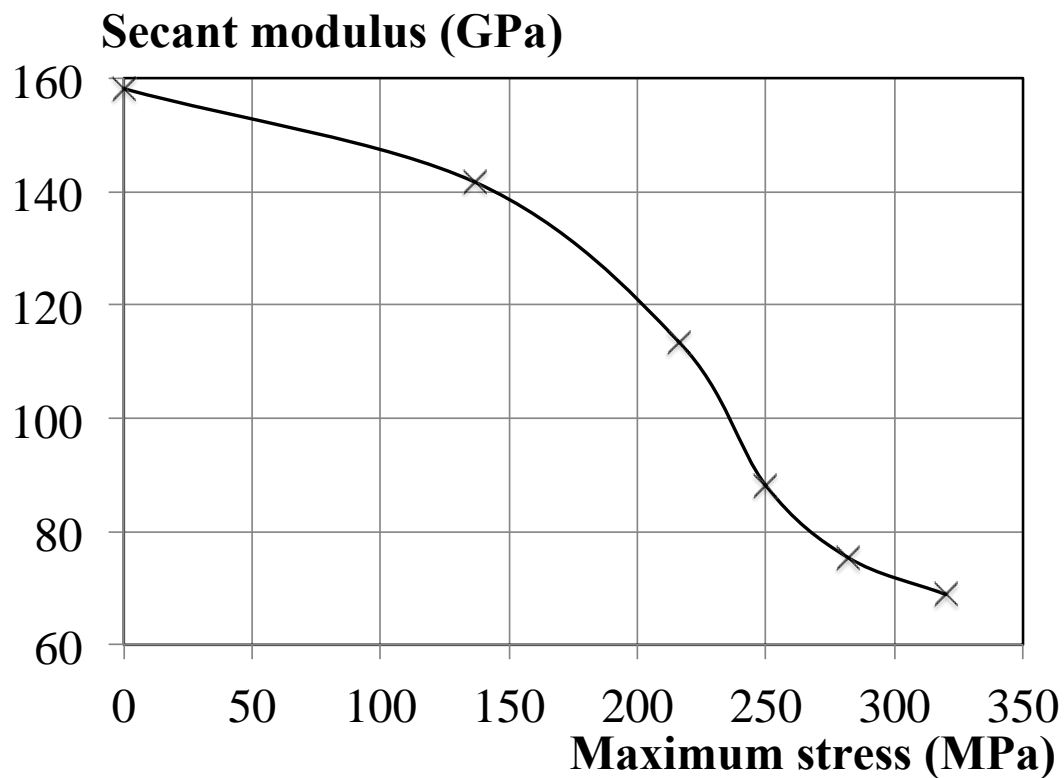
Secant modulus (GPa)

Figure 12. Variation in the secant modulus of the hysteresis loops of a given cycle as a function of the maximum stress imposed to the test piece during this cycle.
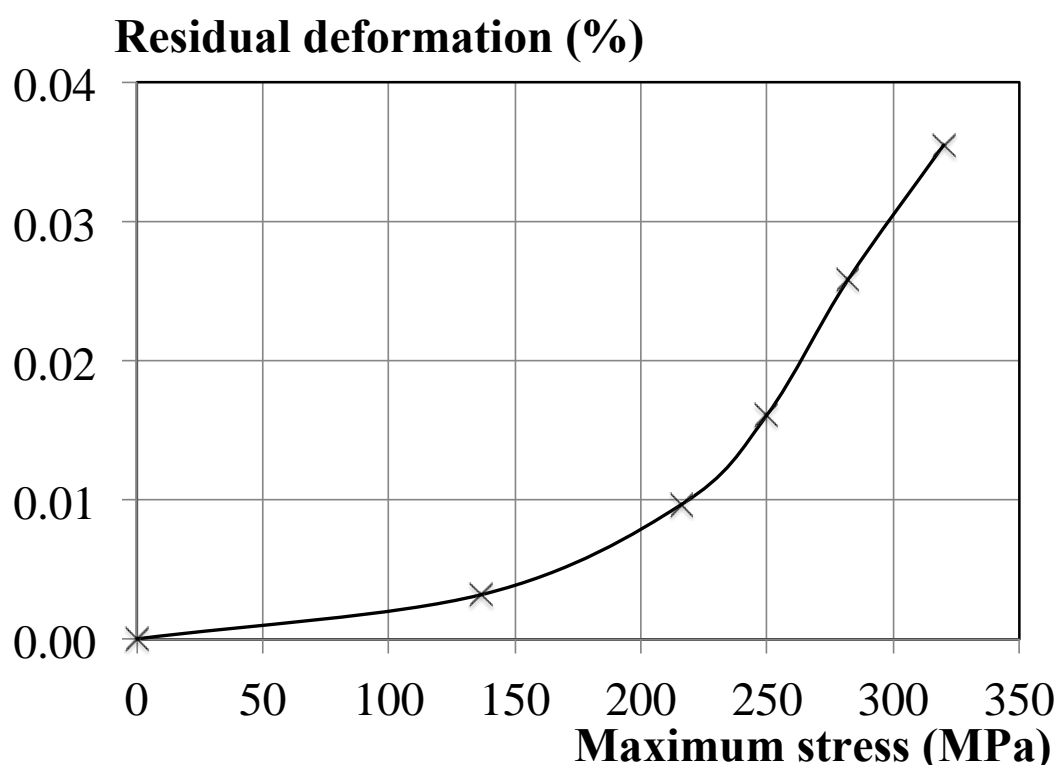
Residual deformation (%)

Figure 13. Variation in the residual deformation as a function of the maximum stress imposed to the test piece.

4. Conclusions

We have checked both the oxidation resistance at high temperature and tensile resistance at room temperature of CMCs densified by Si_2N_2O. These materials, submitted to oxidation in wet oxygen at 1400 °C for 170 h, exhibit an oxidation gradient from the surface to almost the center of the sample. In the outer part of the sample, Si_2N_2O, Si_3N_4 and SiC were oxidized into silica in the cristobalite-crystallized form. The matrix microstructure looks similar to the original one at the center of the sample, while at the surface large pores are observed and the fiber/matrix interphase is consumed by oxidation. The high weight increase observed on the oxidation curves (Figure 6) during the first 20 h of the step temperature at 1400 °C corresponds to the formation of the silica protecting scale. Over longer periods of time, the increase is offset by the vaporization of the silica scale towards an asymptotic value corresponding to a steady state of equilibrium between the formation and the vaporization of the silica layer. The time at which the constant thickness of the silica scale is reached depends on the thickness of the SiC consolidation layer: for the 5-μm-thick SiC layer, the asymptotic value is reached after 40 h. In contrast, because of the greater amount of matrix present in the composite, the silica scale continues to grow till 170 h when the thickness of the SiC consolidation layer is 1 μm. Beyond 170 h, the asymptotic value is almost reached for the sample with a 1-μm-thick consolidation layer. Contrary to our initial hypothesis, which assumed that Si_2N_2O is more resistant to oxidation than SiC or Si_3N_4, our results seem to show that this is not the case, at least in the state of synthesis of this material within our matrix. It is probable that the degree of porosity of the matrix also has an unfavorable influence on its oxidation, whereas the SiC constituting the consolidation layer, which is obtained by CVD, is dense and of better crystallographic quality and consequently resists oxidation better. However, this point requires additional checks. The elastic modulus and the hardness measured at room temperature by nano-indentation are, respectively, 100 and 8 GPa. These data are relatively scattered and low in comparison with the data related to the phases present in the matrix because of the residual porosity caused by the reaction synthesis. The elastic modulus measured at room temperature by the tensile test ranges from 150 to 160 GPa and by the ultimate yield strength from 320 to

390 MPa, which corresponds to a yield strain of about 0.6%. The yield strength identified by acoustic emission is about 40 MPa.

References

1. Naslain, R. Design, preparation and properties of non-oxide CMCs for application in engines and nuclear reactors: An overview. *Compos. Sci. Technol.* **2004**, *64*, 155–170. [CrossRef]
2. Jacobson, N.S.; Myers, D.L. Active Oxidation of SiC. *Oxid. Met.* **2011**, *75*, 1–25. [CrossRef]
3. Brisebourg, M.Q.; Rebillat, F.; Teyssandier, F. Oxidation of β-SiC at high temperature in Ar/O2, Ar/CO2, Ar/H2O gas mixtures: Active/passive transition. *J. Eur. Ceram. Soc.* **2018**, *38*, 4320–4328. [CrossRef]
4. Opila, E.J.; Hann, R.E. Paralinear Oxidation of CVD SiC in Water Vapor. *J. Am. Ceram. Soc.* **1997**, *80*, 197–205. [CrossRef]
5. Du, H.; Tressler, R.E.; Spear, K.E.; Pantano, C.G. Oxidation studies of crystalline CVD silicon Nitride. *J. Electrochem. Soc.* **1989**, *136*, 1527–1536. [CrossRef]
6. Ogbuji, L.U.J.T.; Opila, E.J. A Comparison of the Oxidation Kinetics of SiC and Si_3N_4. *J. Electrochem. Soc.* **1995**, *142*, 925–930. [CrossRef]
7. LOgbuji, U.J.T.; Bryan, S.R. The SiO_2-Si_3N_4 Interface, Part I: Nature of the lnterphase. *J. Am. Ceram. Soc.* **1995**, *78*, 1272–1278. [CrossRef]
8. Ogbuji, L.U.J.T. The SiO_2-Si_3N_4 Interface, Part II: O_2 Permeation and Oxidation Reaction. *J. Am. Ceram. Soc.* **1995**, *78*, 1279–1284. [CrossRef]
9. Fourrier, A.; Bosseboeuf, A.; Bouchier, D.; Gautherin, G. Thermal Oxidation in Wet Oxygen of Reactive Ion-Beam Sputter-Deposited Silicon Nitride Films. *Electrochem. Soc.* **1991**, *138*, 1084–1089. [CrossRef]
10. Washburn, M.E. Silicon oxynitride refractories. *Am. Ceram. Soc. Bull.* **1967**, *46*, 667–671.
11. Lortholary, P.; Goursat, P.; Tétard, D.; Billy, M. Etude du système silicium-oxygène-azote. II de l'oxynitrure Si_2N_2O pulvérulent par l'oxygène au-dessus de 1100 °C. *Rev. Int. Hautes Tempér. Réfract.* **1972**, *9*, 325–332.
12. Persson, J.; Käll, P.O.; Nygren, M. Interpretation of the parabolic and nonparabolic oxidation behavior of silicon oxynitride. *J. Am. Ceram. Soc.* **1992**, *75*, 3377–3384. [CrossRef]
13. Manessis, D.; Du, H.; Larker, R. Oxydation studies of silicon oxynitride ceramics. *J. Electrochem. Soc.* **1998**, *145*, 1355–1360. [CrossRef]
14. Ehlert, T.C.; Dean, T.P.; Billy, M.; Labbe, J.C. Thermal decomposition of the oxynitride of silicon. *J. Am. Ceram. Soc.* **1980**, *63*, 235–236. [CrossRef]
15. Lin, S.; Ye, F.; Ding, J.; Yang, C.P.; Ma, J.; Dong, S.; Liu, Q. Effects of pore diameters on phase, oxidation resistance, and thermal shock resistance of the porous Si_2N_2O ceramics. *J. Am. Ceram. Soc.* **2017**, *100*, 2190–2198. [CrossRef]
16. Lamon, J. A micromechanics-based approach to the mechanical behavior of brittle-matrix composites. *Compos. Sci. Technol.* **2001**, *61*, 2259–2272. [CrossRef]